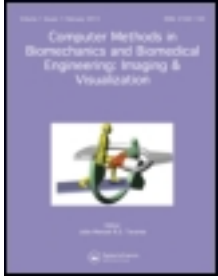


This article was downloaded by: [Universite Paris Dauphine], [Laurent Cohen]

On: 05 March 2013, At: 00:47

Publisher: Taylor & Francis

Informa Ltd Registered in England and Wales Registered Number: 1072954 Registered office: Mortimer House, 37-41 Mortimer Street, London W1T 3JH, UK



Computer Methods in Biomechanics and Biomedical Engineering: Imaging & Visualization

Publication details, including instructions for authors and subscription information:

<http://www.tandfonline.com/loi/tciv20>

Geodesic voting methods: overview, extensions and application to blood vessel segmentation

Youssef Rouchdy^a & Laurent D. Cohen^a

^a CEREMADE, UMR 7534, CNRS, Université Paris Dauphine, 75775, Paris Cedex 16, France

Version of record first published: 04 Mar 2013.

To cite this article: Youssef Rouchdy & Laurent D. Cohen (2013): Geodesic voting methods: overview, extensions and application to blood vessel segmentation, *Computer Methods in Biomechanics and Biomedical Engineering: Imaging & Visualization*, DOI:10.1080/21681163.2013.766019

To link to this article: <http://dx.doi.org/10.1080/21681163.2013.766019>

PLEASE SCROLL DOWN FOR ARTICLE

Full terms and conditions of use: <http://www.tandfonline.com/page/terms-and-conditions>

This article may be used for research, teaching, and private study purposes. Any substantial or systematic reproduction, redistribution, reselling, loan, sub-licensing, systematic supply, or distribution in any form to anyone is expressly forbidden.

The publisher does not give any warranty express or implied or make any representation that the contents will be complete or accurate or up to date. The accuracy of any instructions, formulae, and drug doses should be independently verified with primary sources. The publisher shall not be liable for any loss, actions, claims, proceedings, demand, or costs or damages whatsoever or howsoever caused arising directly or indirectly in connection with or arising out of the use of this material.

Geodesic voting methods: overview, extensions and application to blood vessel segmentation

Youssef Rouchdy¹ and Laurent D. Cohen*

CEREMADE, UMR 7534, CNRS, Université Paris Dauphine, 75775 Paris Cedex 16, France

In this article we present new methods to segment thin tree structures, which are, for example, present in microglia extensions and cardiac or neuronal blood vessels. Many authors have used minimal cost paths, or geodesics relative to a local weighting potential P , to find a vessel pathway between two end points. We use a set of such geodesic paths to find a tubular tree structure with minimal interaction. Recently, we have introduced a set of methods called geodesic voting. In this article, we review all these methods and present some extensions. We also adapt these methods to the segmentation of complex tree structures in a noisy medium and apply them to the segmentation of blood vessels in 2D and 3D.

Keywords: geodesic voting; fast marching; level set; minimal paths; tree structure segmentation

1. Introduction

In this article we present novel methods for the segmentation of tree structures. These methods are based on minimal paths and can be applied to extract numerous structures, such as microglia extensions, neurovascular structures, blood vessels and pulmonary trees. There are many studies dedicated to the extraction of vascular or airway trees. For a review of such methods, see Kirbas and Quek (2004), Lesage et al. (2009), Mori et al. (1996), Agam et al. (2005), Carrillo et al. (2007) and Lo et al. (2010). Among the approaches used to segment such tree structures, we consider the following three models, classified according to their method for extracting the tubular aspect of the tree: centreline-based models, surface models and 4D curve models. The first category focuses on directly extracting the centrelines of the tubular tree (Lorigo et al. 2001; Swift et al. 2002). After extracting the centrelines, a second process can be used to segment the lumen of the tree (see Bouix et al. 2005). The second category directly extracts the surface of the vessel. These approaches include explicit and implicit surface models. The former models use a parametric representation of the tubular structure (Frangi et al. 1999). These models are not adapted to the segmentation of complex tree structures, whereas the latter implicit methods can evolve the surface through complex shape changes including changes in topology (Manniesing et al. 2006; Yan and Kassim 2006). However, initialisation must be carried out carefully to obtain an accurate segmentation.

Minimal path techniques are extensively used for centreline extraction of tubular tree structures. These approaches are robust to the presence of local perturbations due to stenosed branches of the tree or imaging artefacts in which the local image information might be insufficient to guide the shape evolution process. Several minimal path

techniques have been proposed to deal with this problem (Deschamps and Cohen 2000, 2001; Wink et al. 2001; Cohen and Deschamps 2001). These techniques involve designing a metric from the image in such a way that the tubular structures correspond to geodesic paths according to this metric (Cohen and Kimmel 1997). Solving the problem from the practical point of view consists in a front wave propagation from a source point within a vessel, which moves faster along the branches of the vascular tree. These methods require the user to supply a starting point (propagation source) and end points. Each end point results in an extracted minimal path back to the source point. The points located along this minimal path are likely to be located on the vessel of interest. A small amount of work has been devoted to reduce the need for user intervention of the user in the segmentation of tree structure to the initialisation of the propagation from a single point. Gülsün and Tek (2008) defined a stopping criterion based on a 'medialness' measure; the propagation is stopped when 'medialness' drops below a given threshold. This method might suffer from the same problem as region growing because the medialness measure might drop below the given threshold in the presence of lesions or other local image artefacts. Wink et al. (2001) proposed stopping the propagation when the geodesic distance reaches a certain value. However, this method is limited to the segmentation of a single vessel, and the definition of the threshold of the geodesic distance is not straightforward. Cohen and Deschamps (2007) proposed stopping the propagation according to a criterion based on certain geometric properties of the region covered by the front wave. Deschamps and Cohen (2001) assumed that the total length of the tree structure to be visited is roughly given; the stopping criterion is based on the Euclidean length of the minimal path.

*Corresponding author. Email: cohen@ceremade.dauphine.fr

In this article, we present new methods to extract tree structures without using any a priori information and using only a single point provided by the user on the tree structure. The methods are generic, and they can be used to extract any type of tree structure in 2D and in 3D. These methods were presented separately in conferences (Rouchdy and Cohen 2008, 2009, 2011a, 2011b). Here, we provide an overview of all these methods and propose extensions. The approach is based on a completely new concept, namely, geodesic voting. It consists in computing geodesics from a given source point to a set of end points scattered throughout the image. The target structure corresponds to image points with a high-geodesic density. The geodesic density is defined at each pixel of the image as a number of geodesics pass over this pixel. Because the potential exhibits low values along the tree structure, geodesics will preferably migrate towards this structure and thereby yield a high-geodesic density. We introduce different approaches to segment complex tree structures in noisy media environments and apply them to segment blood vessels in medical images.

In Section 2, we introduce the geodesic voting approach. In Section 3, we propose a variety of possible ways to obtain both the centreline and the boundary of the vascular tree. In Section 4, we evaluate the method on 2D retinal images.

2. Background

2.1 Minimal paths

In the context of image segmentation proposed by Cohen and Kimmel (1997), a deformable model to extract contours between two points was given by the user. The model is formulated to find a geodesic for a weighted distance:

$$\min_y \int_0^L (w + P(y(s))) ds, \quad (1)$$

the minimum is considered over all curves $y(s)$ traced on the image domain Ω that links the two end points, that is $y(0) = x_0$ and $y(L) = x_1$. The constant w imposes regularity on the curve. $P > 0$ is a potential cost function computed from the image; it takes lower values near the edges or the features. For instance, $P(y(s)) = I(y(s))$ leads to darker lines, whereas $P(y(s)) = g(\|\nabla I\|)$ leads to the edges, where I is the image and g is a decreasing positive function.

To compute the solution associated with the source x_0 of this problem, Cohen and Kimmel (1997) proposed a Hamiltonian approach and found the geodesic weighted distance U that solves the Eikonal equation, $\|\nabla U(x)\| = w + P(x)$, $\forall x \in \Omega$. The ray y is subsequently computed by back-propagation from the end point x_1 by

solving the ordinary differential equation:

$$y'(s) = -\nabla U(y). \quad (2)$$

The idea behind the fast marching algorithm is to propagate the wave in only one direction, starting with the smaller values of the action map U and progressing to the larger values using the upwind property of the scheme. Therefore, the fast marching method permits to solve the Eikonal in complexity $O(n \log(n))$ (for details, see Cohen and Kimmel 1997).

2.2 Geodesic voting for the segmentation of tree structures

In Rouchdy and Cohen (2008), we have introduced a new concept to segment a tree structure from only one point given by the user in the tree structure. This method consists in computing the geodesic density from a set of geodesics extracted from the image. Assume we are looking for a tree structure for which a potential cost function has been defined as above and has lower values on this tree structure. First, we provide a starting point x_0 roughly at a root of the tree structure, and we propagate a front wave in the whole image with the fast marching method, obtaining the minimal action U . Then we consider an end point anywhere in the image. Backtracking the minimal path from the end point, we will reach the tree structure somewhere and stay on it until the start point is reached. So, a part of the minimal path lies on some branches of the tree structure. The idea of this approach is to consider a large number of end points $\{x_k\}_{k=1}^N$ on the image domain and to analyse the set of minimal paths y_k obtained. For this, we consider a voting scheme along the centrelines. When backtracking each path, we add 1 to each pixel we pass over. At the end of this process, pixels on the tree structure will have a high vote because many paths have to pass over it. On the contrary, pixels in the background will generally have a low vote because very few paths will pass over them. The result of this voting scheme is what we call the geodesic density or voting score. This means at each pixel the density of geodesics pass over this pixel. The tree structure corresponds to the points with high-geodesic density.

We define the voting score or the geodesic density at each pixel p of the image by

$$\mu(p) = \sum_{k=1}^N \delta_p(y_k), \quad (3)$$

where the function $\delta_p(y)$ returns 1 if the path y crosses the pixel p , else 0. Once the geodesic voting is made, the tree structure is obtained by a simple thresholding of the geodesic density μ . As shown in Rouchdy and Cohen (2011a) and Figure 1, the contrast between the background and the tree is large, and the threshold can be chosen easily.

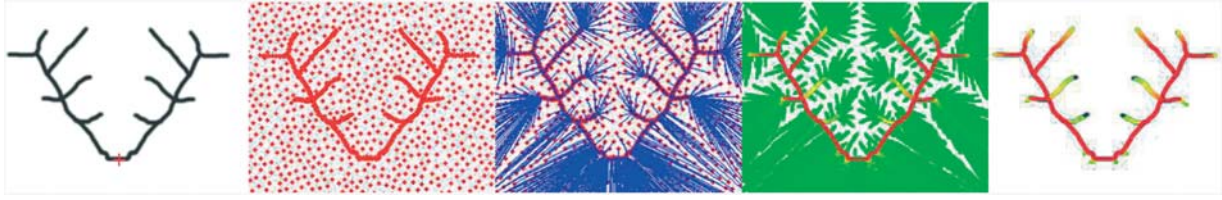


Figure 1. Geodesic voting method. From left to right: the first panel shows the synthetic tree, and the red cross represents the root of the tree; the second panel shows the adaptive set obtained from the farthest point strategy, described by Rouchdy and Cohen (2009); the third panel shows the geodesics extracted from the adaptive set of points to the root, in blue; the fourth panel shows the geodesic density; the fifth panel shows the geodesic density after thresholding.

The set of end points for which we consider the geodesics can be defined through different choices. This could be all pixels over the image domain, random points, scattered points according to some criterion, or simply the set of points on the boundary of the image domain. Taking only the points on the boundary of the image domain misses some branches of the tree as explained in Rouchdy and Cohen (2009). Considering all the points of the image has the advantage that no possible paths are lost and that the scores are smoothed, but it increases the computation time and makes the thresholding more difficult. About computation of paths, the transport equation approach of Section 2.3 is not dependant on the number of end points, and thus is useful when it is needed to consider a large number of end points. A good trade-off for the choice of end points is the adaptive set proposed in Rouchdy and Cohen (2009), which can be viewed as a random set of points scattered all over the image with a higher density where the potential P is smaller (see Figure 1).

2.3 Voting with a transport equation

The geodesic voting can be obtained in a different manner without computing the minimal paths. The trajectories y_k computed from Equation (2) are called characteristics for the conservation equation

$$u_t + \operatorname{div}(vu) = 0, \quad (t, x) \in]0, T[\times \Omega, \quad (4)$$

where $v = -\nabla U$ denotes the velocity field computed from the distance map U . Because of the conservation of the information transported by Equation (4) towards the source

point, we can define geodesic density as the integral of the solution of the transport Equation (4) in time T

$$\mu(x) = \int_0^T u(t, x) dt. \quad (5)$$

The initial conditions in the transport formulation of the geodesic voting determine the set of end points used to extract the geodesics in the original formulation of the geodesic voting, presented previously. Here, we take initial condition $u(0, \cdot) = 1$ in the interior of the image domain. A non-null value for the initial condition in a given image point means that a geodesic is extracted from this point, whereas the value 0 means that no geodesic is extracted.

Integrating of the transport Equation (4) with respect to time t we get

$$\operatorname{div}(v\mu) = u(0, x) - u(T, x), \quad x \in \Omega. \quad (6)$$

The partial differential Equation (6) is not elliptic, so it is more convenient to compute the geodesic density by relation (5) after solving the transport Equation (4). Figure 2 shows the segmentation result obtained with this scheme. We have considered a simple synthetic image representing a tree structure like deer woods (see Figure 2, left). The pixels with high density correspond to the structure extracted from the image (see Figure 2, right).

3. Geodesic voting methods for blood vessel segmentation

The geodesic voting method gives a good approximation of the localisation of the tree branches, but it does not

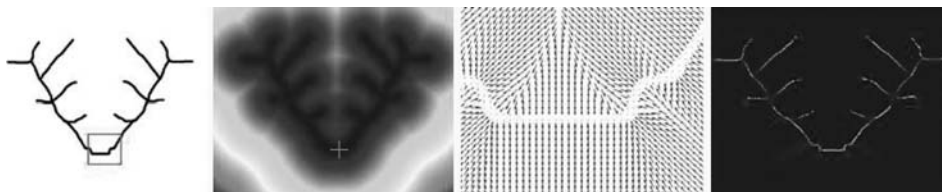


Figure 2. Voting by transport equation. First panel: synthetic image representing a tree structure. Second panel: distance map, the source point is indicated by a red cross. Third panel: zoom on the velocity field shown in the region indicated by a red square in the first panel. Fourth panel: geodesic density computed by relation (6).

allow to extract the tubular aspect of the tree. Here, we extend the geodesic voting to the segmentation of the boundary of the tubular structure.

3.1 Geodesic voting in an augmented space

In this section, we introduce a constraint that ensures that the segmented tree approximates well the centrelines of the tree, and we adapt the geodesic voting method to segment the walls of the tubular tree structure. The idea is to carry out the geodesic voting with a potential that integrates an extra dimension used to measure the distance from the centreline to the walls of the vessels. The potential proposed by Li and Yezzi (2007) incorporates this measure. More precisely, this potential is defined by $\tilde{P} : (x, r) \in \Omega \times [0, r_{\max}] \rightarrow \tilde{P}(x, r)$. It incorporates the full set of image values within the sphere of centre x and radii r , and it is designed in such a way that the whole sphere lies inside the desired object and is as large as possible so that it is tangential to the boundary of the object. The extension of the minimal path extraction model (1) to the case of a

potential with an extra dimension is achieved by minimising the following energy:

$$\min_{c,r} \int_0^t (\omega + \tilde{P}(c(s), r(s))) ds. \quad (7)$$

The minimisation of this energy allows simultaneous approximation of the minimal path and the radii of the spheres tangent to the boundary of the tube with centres located along the minimal path. The computation of the path is achieved with the framework presented in Section 2.1 in a space augmented with an extra dimension, being the radius.

Using potential \tilde{P} and a set of end points (x_k, r_k) (uniform grid) in the domain, we extract a set of geodesics y_k from which we compute the geodesic density $(x, r) \rightarrow \mu(x, r)$ given by Equation (3). In this case, the geodesic voting map is a function of the spatial dimension and also of the radii of the spheres. There are many ways to use this (3D + radius) geodesic density to extract the tree structure (Rouchdy and

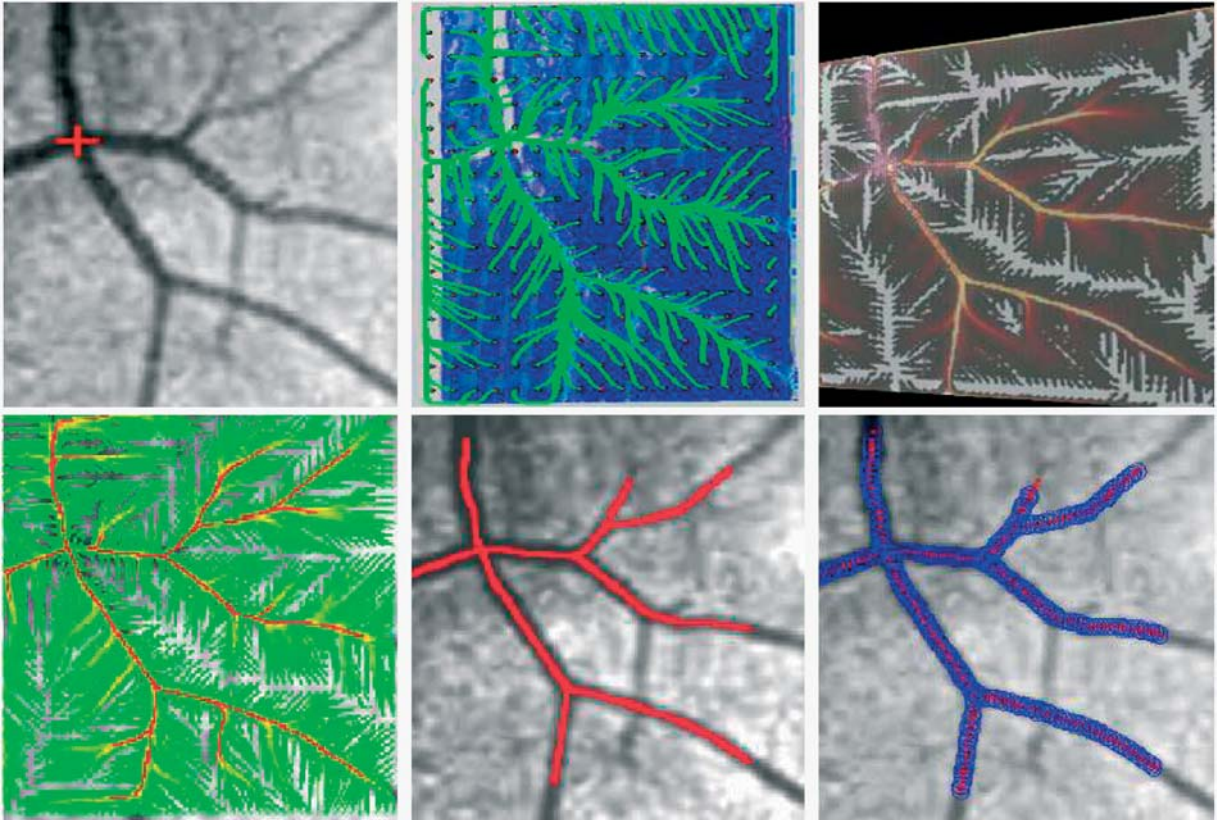


Figure 3. Vessel segmentation for a 2D retinal image with the geodesic voting method in augmented space. First row: the left panel shows a 2D retinal image, the red cross indicates the source point; the centre panel shows, in $(2D + \text{radius})$ domain, in green the paths extracted from a uniform grid to the source point; the right panel shows the density computed in $(2D + \text{radius})$ domain, yellow colour corresponds to high density and brown to low density. Second row: the left panel shows the geodesic density $\tilde{\mu}_m$, given by Equation (8), red colour corresponds to high density, yellow colour to medium and green colour to low density; the centre panel shows the density $\tilde{\mu}_m$ after thresholding in red; the right panel in blue shows the extraction result of the tubular structure obtained by thresholding the map $\{\tilde{\mu}_m, \tilde{r}\}$, where $\tilde{r}(x) = \arg \max_{r \in [0, r_{\max}]} \tilde{\mu}_m(x, r)$.

Cohen 2011a). Here, we use the following spatial density:

$$\tilde{\mu}_m(x) = \sum_{r=0}^{r_{\max}} \mu(x, r). \quad (8)$$

Figure 3 illustrates the steps of this method for the segmentation of the tubular aspect of the tree. We can see the efficiency of the method to obtain a segmented tree that is centred in the structure, as well as the precise boundary of the vascular tree.

3.2 Geodesic voting shape prior to constrain the level set evolution

Here, we present a second approach to extract the walls of the vessels using the original geodesic voting method. A shape prior constraint is constructed from the geodesic voting tree to constrain the evolution of a level set active contour to extract the walls of the tree. As illustrated in Rouchdy and Cohen (2011b) and in Section 4, a level set approach on this kind of images, even with the initialisation obtained from the geodesic voting, is inefficient because the background region is not homogeneous. A Bayesian approach is used to introduce this shape prior into the level set formulation. The model is formulated as a minimisation problem of a global energy composed of two terms. The first term corresponds to deformation energy for a standard region-based level set method and the second term introduces the shape prior:

$$E_b(\phi, c_1, c_2) = \mathcal{V}(\phi, c_1, c_2) + \frac{\gamma}{2\sigma^2} \int_{\Omega} (\phi - \tilde{\phi})^2 \delta_{\varepsilon}(\phi) dx, \quad (9)$$

where the factor term δ_{ε} allows us to restrict the shape prior within the region of interest, and $\tilde{\phi}$ is the signed distance computed from the geodesic voting tree. The segmentation of vessels with this approach is achieved in two steps: (1) the geodesic voting tree is extracted using the original geodesic voting method (2) the walls of the vessels are extracted by minimisation of the functional E_b . Figure 4 illustrates the segmentation process. Details about this method are given in Rouchdy and Cohen (2011b).

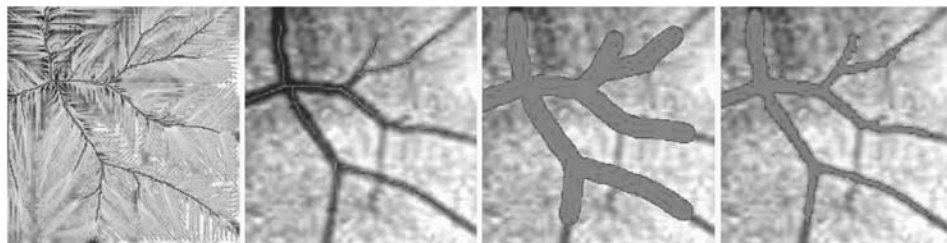


Figure 4. Geodesic voting shape prior segmentation of vessels from a 2D retinal image. From left to right: adaptive voting on the image, voting tree obtained by thresholding the geodesic voting, shape prior obtained by dilation of the voting tree, segmentation result obtained with region-based active contour with shape prior (method described in Section 3.2).

3.3 The deformable band and tube

The deformable band and tube methods, proposed by Mille and Cohen (2009), combine aspects of region-based active contours and minimal paths. It is devoted to the recovery of tubular structures. In this context, the segmentation process is constrained by essence, rather than by adding shape prior terms in a general model, as in Section 3.2. In 2D, the band is defined by an open curve Γ , parameterised by arc length $s \in [0, 1]$, and radius function $\mathcal{R} : [0, 1] \rightarrow \mathbb{R}^+$. Curve Γ plays the role of the medial axis. The inner region R_{in} of width $2\mathcal{R}$ is bounded by curves $\Gamma_{[\mathcal{R}]}$ and $\Gamma_{[-\mathcal{R}]}$, constructed by translating Γ both ways along normal n by length \mathcal{R} .

The band is endowed with energy functional E , weighted sum of the internal energy E_{smooth} and the external region energy E_{data} :

$$E(\Gamma, \mathcal{R}) = \omega E_{\text{smooth}}(\Gamma, \mathcal{R}) + (1 - \omega) E_{\text{data}}(\Gamma, \mathcal{R}). \quad (10)$$

The user-provided coefficient ω , weighting the influence of E_{smooth} over E_{data} , controls the elastic properties of the deformable band. The smoothness energy E_{smooth} is expressed in terms of curve length and radius first order derivative. Because the structure of interest should satisfy an intensity homogeneity criterion, the data term is as follows:

$$E_{\text{data}}(\Gamma, \mathcal{R}) = \int_{R_{\text{in}}} g_{\text{in}}(x) dx + \int_{R_{\text{out}}} g_{\text{out}}(x) dx, \quad (11)$$

where region descriptors g_{in} and g_{out} increase with respect to intensity inhomogeneity. The initial curve Γ is built using the geodesic voting method.

The 3D extension to deformable tube approach is described in Mille and Cohen (2009), and Figures 5 and 6 depict results obtained on a computed tomography (CT) volume data, starting deformation from the result of the geodesic voting tree. Figure 6(right) represents a slice of the CT data, with centrelines and surface positions of two segments (aorta and superior mesenteric artery). With a C++ implementation running on an Intel Core 2 Duo 2.2 GHz PC (4 GB RAM) (Intel Corporation), computational cost for a $256 \times 256 \times 256$ volume image is 28 s for extracting the surface, see the result in Figure 5. According to

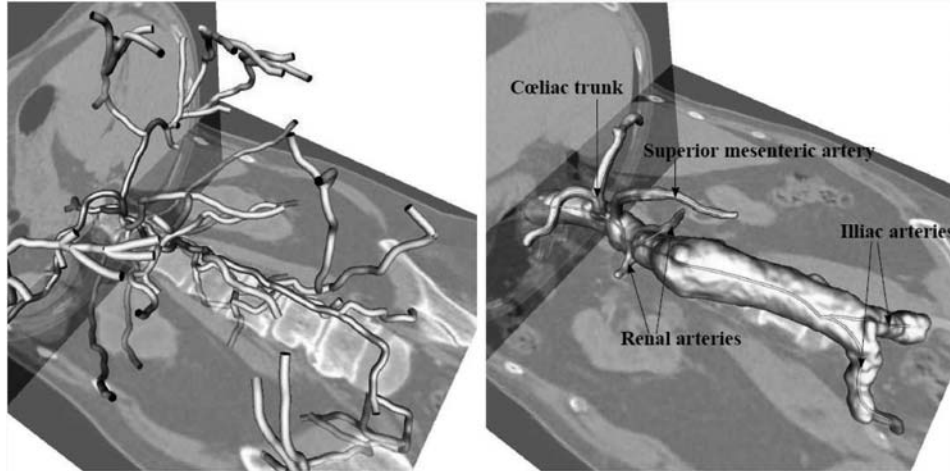


Figure 5. Deformable tube model: on the left, tree after thresholding on geodesic voting score; on the right, final tree with boundary surface (from Mille and Cohen 2009).

visual inspection, we believe the reconstruction results to be promising.

4. Results and discussion

In this section, we compare GVR (Geodesic Voting with Radius), method with radius presented in Section 3.1, and GVP (Geodesic Voting Prior), method with shape prior presented in Section 3.2, with other approaches [the edge-based level set method (Malladi et al. 1995), the Chan and Vese (2001) method and the fuzzy connectedness method (Udupa et al. 2002)] for vessel segmentation from retinal images on the digital retinal images for vessel extraction (DRIVE) data (Staal et al. 2004).

The DRIVE data were acquired using a Canon CR5 non-mydiatic 3CCD camera with a 45° field of view (FOV). Each image was captured using 8 bits per colour plane at 768

by 584 pixels. The FOV of each image is circular with a diameter of approximately 540 pixels. For this database, the images have been cropped around the FOV. The DRIVE data are composed of 40 images from different subjects for which manual segmentations are also provided.

Considering the complexity of the retinal images and the properties of our algorithm, we have cropped 12 different images from the 40 images available and made validation of our method on them. Note that the retinal vessels in each image do not correspond to a tree structure. Some images may contain several disconnected trees or networks. Note that when the image contains more than one tree structure, the geodesic voting method tends to create connections between them. These connections may not make sense anatomically; therefore, a preprocessing or post-processing step is necessary to get an accurate segmentation. For a completely automated application,

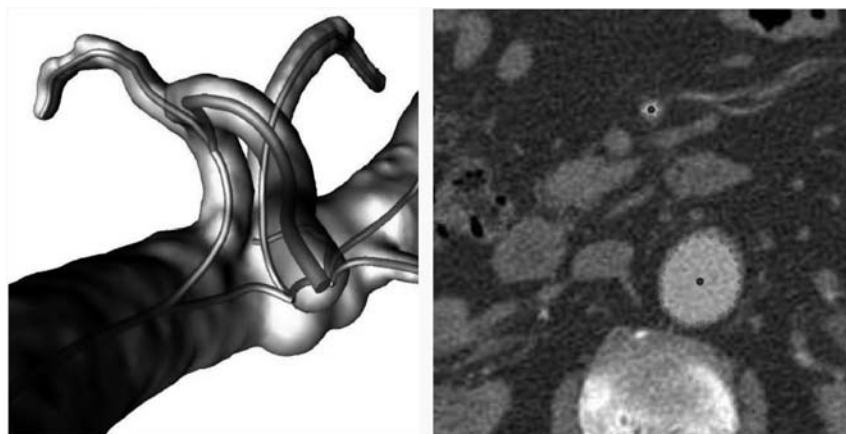


Figure 6. Deformable tube model: a closer look at the boundary surface. On the left, a representation with centerlines; on the right, slice of the 3D CT image, with centerlines and surface positions of two segments: aorta (bottom) and superior mesenteric artery (top) (from Mille and Cohen 2009).

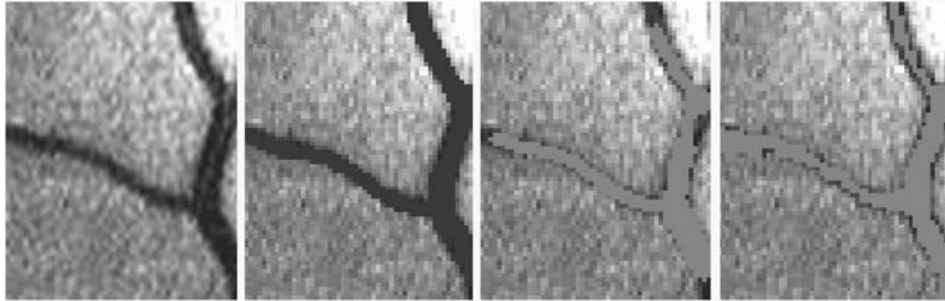


Figure 7. Blood vessels segmentation using the GVR and GVP methods from one of the 12 cropped retinal images (DRIVE data). The left panel shows the original image, the second panel shows the manual segmentation in blue, the third panel shows the segmentation result obtained with the GVR method, the right panel shows the segmentation result obtained with the GVP method.

this problem may be solved by using the selection step proposed (for a different method) in Rouchdy et al. (2011) to remove paths that are unlikely to belong to the microglia extensions. This is out of focus of this article to propose precise automatic pre- or post-processing to deal with all kind of situations. Therefore, it was more illustrative to choose images that contain tree structures and then crop the image in such a way that the cropped image contains only one tree structure. We were able to extract 12 tree structures from 12 different images in the DRIVE data. The size of the cropped image depends on the size of the tree in the original image and on average corresponds to 100 pixels in height and 50 pixels in width.

For the GVR method, the augmented potential \tilde{P} used is described in Section 3.1. The starting point was chosen as a junction of the tree. As the end points were chosen as a uniform grid, the spatial starting point can be chosen anywhere within the tree. However, the starting radii should be chosen carefully to get an optimal segmentation. In our experiments on DRIVE data, we obtained good estimation of these parameters by testing different values following the study presented by Li and Yezzi (2007). These parameters can be optimised and automated for a given class of images.

For the GVP method, we have used the following potential $P(x) = I(x)^3$ to run the geodesic voting segmentation, where I is the greyscale intensity of the image. The value of γ , the weight on the shape prior, was chosen empirically and used for all the experiments presented in the article. We

showed in Rouchdy and Bloch (2011) that this value can be chosen in a large range with the same efficiency.

In Figures 7 and 8 (results obtained with the GVR and GVP), the source point used to carry out the geodesic voting was chosen empirically on the junction of the tree that is connected to the largest number of branches. This allows us to segment the largest number of branches in the presence of small branches with weak contrast. Note that the quality of the images provided by DRIVE is not very good, and sometimes it is hard to set optimal sphere radii for the GVR initialisation. When it is not possible to give a precise radius, we underestimate the value of the radius whenever possible; indeed, we measure the radii of the spheres in pixels, and their diameters are odd numbers. Concerning the end points, we have used the same number for each method: 1200 farthest points (generated by the process described in Rouchdy and Cohen 2009) for the GVP method and a uniform grid of the augmented potential for the GVR method. The threshold for the geodesic density was defined from the first five images as the mean value of all the threshold values manually selected for these five images. Then this mean threshold was used for all the 12 images. We have used two different values for the mean threshold: one value for the GVP method and the other for the GVR method.

In Rouchdy and Cohen (2012), we compare the GVR and GVP results for vessel segmentation on the DRIVE database in terms of the following evaluation measures:

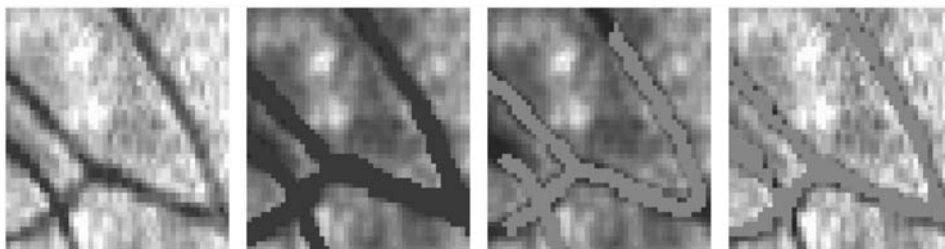


Figure 8. Blood vessels segmentation using the GVR and GVP methods from one of the 12 cropped retinal images (DRIVE data). The left panel shows the initial image, the second panel shows the manual segmentation in blue, the third panel shows the segmentation obtained with GVR method, in red, the right panel shows the segmentation obtained with our GVP method.

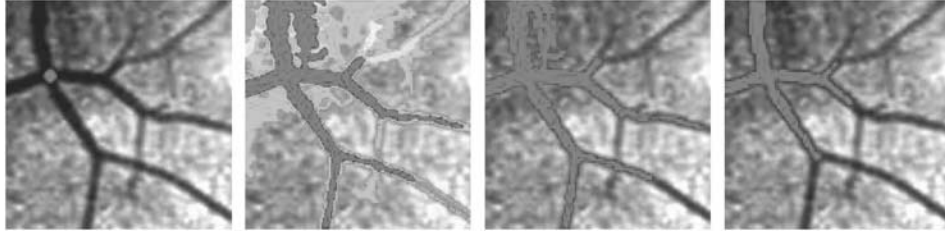


Figure 9. Fuzzy connectedness segmentation. The panels show from the left to the right: the localisation of the red seed point, the fuzzy connectedness map, the thresholded fuzzy connectedness map with the threshold set at th_1 (third panel), the thresholded fuzzy connectedness map with a threshold set at th_2 superior to th_1 .

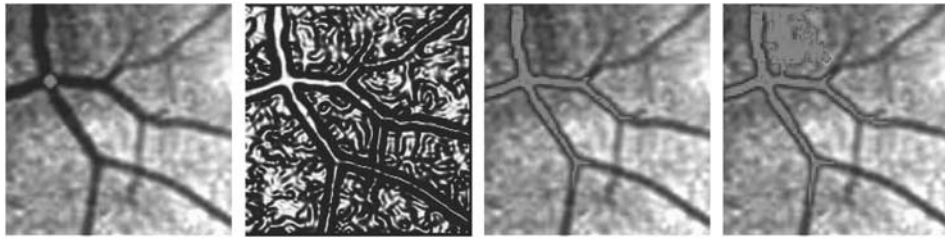


Figure 10. Edge-based level set method. The left panel shows (in red) the initial position of the interface, second panel shows the sigmoid of the gradient magnitude, the third panel shows the interface after 1000 iterations, the right panel shows the interface after 2000 iterations.

dice, specificity and sensitivity. We found that GVR and GVP gave similar results.

In the sequel, we compare the performance of GVR and GVP methods with the edge and region-based level set methods and the fuzzy connectedness method in the segmentation of vessels.

Figure 9 shows the results obtained with the fuzzy connectedness method (Udupa et al. 2002). The segmentation of the tree is obtained by thresholding the fuzzy connectedness map. For a small threshold, the method does not allow us to extract all the branches of the tree, and when the threshold is increased, the propagation leaks outside of the tree. The same problems were observed with the edge-based level set method (Malladi et al. 1995) when we increased the number of iterations, see Figure 10. The shape prior allows us to constrain the propagation inside the tubular tree. Figure 11 shows that the propagation

without shape constraints ($\gamma = 0$ in Equation (9)) can leak outside of the tree structure.

Our methods (GVP and GVR) give the best results: they succeed in segmenting more tree branches without leaking outside of the tree structures.

5. Conclusion

In this article, we have presented a completely new approach for the segmentation of tree structures based on geodesic voting. This approach is adapted to automatically segment tree structures from a single point provided by the user with no further a priori information required about the tree. By contrast, other methods described in the literature for the segmentation of tree structures are not fully automatic and require shape prior information about the tree to be segmented. We have combined this approach

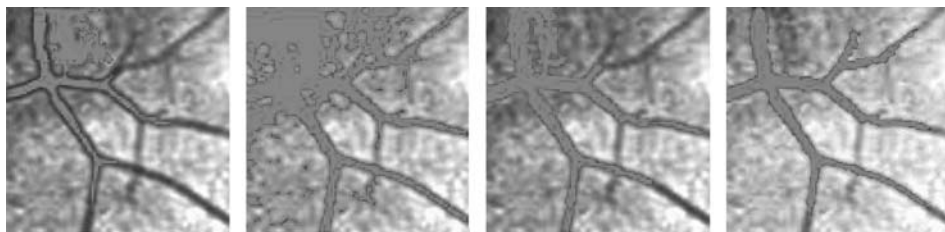


Figure 11. Comparison of the geodesic voting approach (GVP) with other methods. The left panel shows (in red) the segmentation obtained by edge-based level set method, the second panel shows (in red) the segmentation results obtained with a Chan and Vese method without using the geodesic voting shape prior, the third panel shows the fuzzy connectedness segmentation, the right panel shows the segmentation result obtained with our geodesic voting with shape prior (GVP).

with an added fourth dimension (space + radius) or with region-based level sets using shape priors to obtain both the centrelines and boundaries of the tree. We have applied our geodesic voting approach to segment different tree structures from a variety of biomedical images. Finally, we have evaluated our approach on retinal 2D images and have shown segmentation results on 3D data. The results were satisfying and promising.

Acknowledgement

The authors would like to thank Julien Mille for his collaboration to combine the geodesic voting and the deformable band methods. This work was partially supported by ANR grant MESANGE ANR-08-BLAN-0198.

Note

¹ Email: cohen@ceremade.dauphine.fr

References

- Agam G, Armato SG, III, Wu C. 2005. Vessel tree reconstruction in thoracic CT scans with application to nodule detection. *IEEE Trans Med Imaging*. 24(4):486–499.
- Bouix S, Siddiqi K, Tannenbaum A. 2005. Flux driven automatic centerline extraction. *Med Image Anal*. 9(3):209–221.
- Carrillo J, Hernández Hoyos M, Davila-Serrano E, Orkisz M. 2007. Recursive tracking of vascular tree axes in 3D medical images. *Int J Comput Assist Radiol Surg*. 1(6):331–339.
- Chan TF, Vese LA. 2001. Active contours without edges. *IEEE Trans Med Imaging*. 10(2):266–277.
- Cohen LD, Deschamps T. 2001. Multiple contour finding and perceptual grouping as a set of energy minimizing paths. In: *Proceedings of Third International Conference on Energy Minimization Methods in Computer Vision and Pattern Recognition (EMMCVPR – 2001)*. Springer Lecture Notes in Computer Science 2134, Sophia-Antipolis, France. p. 560–575.
- Cohen LD, Deschamps T. 2007. Segmentation of 3D tubular objects with adaptive front propagation and minimal tree extraction for 3D medical imaging. *Math Models Methods Appl Sci*. 10(4):289–305.
- Cohen LD, Kimmel R. 1997. Global minimum for active contour models: a minimal path approach. *Int J Comput Vis*. 24(1):57–78.
- Deschamps T, Cohen LD. 2000. Minimal paths in 3D images and application to virtual endoscopy. In: *Sixth European Conference on Computer Vision ECCV(2)*. Dublin, Ireland: Springer-Verlag Berlin Heidelberg. p. 543–557.
- Deschamps T, Cohen LD. 2001. Fast extraction of minimal paths in 3D images and applications to virtual endoscopy. *Med Image Anal*. 5(4):281–299.
- Frangi AF, Niessen WJ, Hoogeveen RM, van Walsum T, Viergever MA. 1999. Model-based quantitation of 3D magnetic resonance angiographic images. *IEEE Trans Med Imaging*. 18(10):946–956.
- Gülsün MA, Tek H. 2008. Robust vessel tree modeling. In: *MICCAI (1)*. New York, NY: Springer-Verlag Berlin Heidelberg. p. 602–611.
- Kirbas C, Quek F. 2004. A review of vessel extraction techniques and algorithms. *ACM Comput Surv*. 36(2):81–121.
- Lesage D, Angelini ED, Bloch I, Funka-Lea G. 2009. A review of 3D vessel lumen segmentation techniques: models, features and extraction schemes. *Med Image Anal*. 13(6):819–845.
- Li H, Yezzi A. 2007. Vessels as 4D curves: global minimal 4D paths to extract 3D tubular surfaces and centerlines. *IEEE Trans Med Imaging*. 26:1213–1223.
- Lorigo L, Faugeras O, Grimson W, Keriven R, Kikinis R, Nabavi A, Westin C-F. 2001. Curves: curve evolution for vessel segmentation. *Med Image Anal*. 5:195–206.
- Lo P, Sparring J, Ashraf H, Pedersen JJH, de Bruijne M. 2010. Vessel-guided airway tree segmentation: a voxel classification approach. *Med Image Anal*. 14(4):527–538.
- Malladi R, Sethian JA, Vemuri BC. 1995. Shape modeling with front propagation: a level set approach. *IEEE Trans Pattern Anal Mach Intell*. 17(2):158–175.
- Manniesing R, Velthuis BK, van Leeuwen MS, van der Schaaf IC, van Laar PJ, Niessen WJ. 2006. Level set based cerebral vasculature segmentation and diameter quantification in CT angiography. *Med Image Anal*. 10(2):200–214.
- Mille J, Cohen L. 2009. Deformable tree models for 2D and 3D branching structures extraction. In: *Computer Vision and Pattern Recognition Workshop on Mathematical Methods in Biomedical Image Analysis (MMBIA)*. 2009 June 20–25 Miami, FL: IEEE. p. 149–156.
- Mori K, Hasegawa J, Toriwaki J, Anno H, Katada K. 1996. Recognition of bronchus in three-dimensional X-ray CT images with application to virtualized bronchoscopy system. In: *Pattern Recognition, 13th International Conference*. 1996 Aug 25–29, IEEE. p. 528–532.
- Rouchdy Y, Bloch I. 2011. A chance-constrained programming level set method for longitudinal segmentation of lung tumors in CT. *Conf Proc IEEE Eng Med Biol Soc*. 2011:3407–3410.
- Rouchdy Y, Cohen LD. 2008. Image segmentation by geodesic voting. application to the extraction of tree structures from confocal microscope images. In: *The 19th International Conference on Pattern Recognition*. Tampa, FL: IEEE. p. 1–5.
- Rouchdy Y, Cohen LD. 2009. The shading zone problem in geodesic voting and its solutions for the segmentation of tree structures. application to the segmentation of microglia extensions. In: *MMBIA 2009: IEEE Computer Society Workshop on Mathematical Methods in Biomedical Image Analysis in conjunction with CVPR'09*. Miami, FL: IEEE Computer Society. p. 66–71.
- Rouchdy Y, Cohen LD. 2011a. A geodesic voting method for the segmentation of tubular tree and centerlines. In: *Eighth IEEE International Symposium on Biomedical Imaging (ISBI'11)*. Chicago, IL: IEEE. p. 979–983.
- Rouchdy Y, Cohen LD. 2011b. A geodesic voting shape prior to constrain the level set evolution for the segmentation of tubular trees. In: *Third International Conference on Scale Space and Variational Methods in Computer Vision (SSVM)*. Ein-Gedi, Israel: Springer. p. 1–12.
- Rouchdy Y, Cohen LD. 2012. Retinal blood vessel segmentation using geodesic voting methods. In: *9th IEEE International Symposium on Biomedical Imaging: From Nano to Macro*. ISBI 2012; 2012 May 2–5 Barcelona, Spain: IEEE. p. 744–747.
- Rouchdy Y, Cohen LD, Pascual O, Bessis A. 2011. Minimal path techniques for automatic extraction of microglia extensions. *Int J Comput Vis Biomech*. 4(1):35–42.
- Staal J, Abramoff M, Niemeijer M, Viergever M, van Ginneken B. 2004. Ridge based vessel segmentation in colour images of the retina. *IEEE Trans Med Imaging*. 23(4):501–509.
- Swift RD, Kiraly AP, Sherbondy AJ, Austin AL, Hoffman EA, McLennan G, Higgins WE. 2002. Automatic axis generation

- for virtual bronchoscopic assessment of major airway obstructions. *Comput Med Imaging Graph.* 26(2):103–118.
- Udapa JK, Saha PK, de Alencar Lotufo R. 2002. Relative fuzzy connectedness and object definition: theory, algorithms, and applications in image segmentation. *IEEE Trans Pattern Anal Mach Intell.* 24(11):1485–1500.
- Wink O, Niessen NJ, Verdonck B, Viergever MA. 2001. Vessel axis determination using front wave propagation analysis. In: MICCAI'01 Proceedings of the 4th International Conference on Medical Image Computing and Computer-Assisted Intervention; 2001. London: Springer-Verlag. p. 845–853.
- Yan P, Kassim AA. 2006. Segmentation of volumetric MRA images by using capillary active contour. *Med Image Anal.* 10(3):317–329.